Received: 7 July 2020 | Revised: 27 August 2020 | Accepted: 11 September 2020

DOI: 10.1002/ppap.202000139

FULL PAPER

PLASMA PROCESSES AND POLYMERS

Detection of long-lived species in plasma-activated water, based on digital colorimetry

Zhenping Zou | **Rui Han** | **Chen Lu** | **Zilan Xiong**

State Key Laboratory of Advanced Electromagnetic Engineering and Technology, Huazhong University of Science and Technology, Wuhan, Hubei, China

Correspondence
Zilan Xiong, State Key Laboratory of Advanced Electromagnetic Engineering and Technology, Huazhong University of Science and Technology, Wuhan, 430074 Hubei, China.
Email: zilanxiong@hust.edu.cn

Funding information
Independent Innovation Fund of Huazhong University of Science and Technology, Grant/Award Number: 2018KFYYXJJ071; National Natural Science Foundation of China, Grant/Award Number: 51907076

Abstract

To fit a specific application, a cheap and effective manner of measurement of chemistries in plasma-activated water (PAW) is in demand. We propose a digital colorimetry-based method of quantifying the long-lived species in PAW using only smartphones and specialized software. Pin–plate discharge and surface microdischarge were used to generate the PAWs. H_2O_2 and NO_2^- were selected as representatives for the test. Various color parameters were extracted from images of a solution consisting of testing species and colorimetric reagent. Specialized curve-fitting strategies were developed during data processing. The results were consistent with those measured by UV–Vis spectrometry, but they provided better performance and simplified operation. Additionally, the proposed PAW generator design can be integrated with the detecting module based on this method.

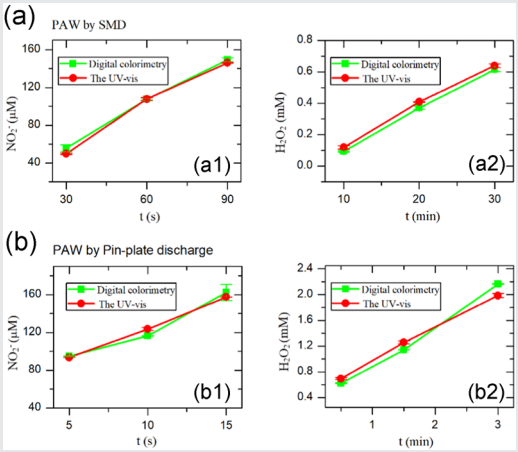

1 | INTRODUCTION

Due to its complex physical and chemical composition, atmospheric-pressure plasma has great potential in various fields, including biomedicine, material modification, and green agriculture.[1–6] Research on the nature of plasma and its interaction with substrates could provide a fundamental understanding of the theoretical basics, which could be utilized in practical applications. Accurate diagnostics of the reactive species and their physicochemical processes is particularly important in plasma fundamental research. Therefore, researchers have been developing various detection methods for plasma diagnosis.[7–12] For example, using absorption spectroscopy, Bruggeman et al.[8] measured the absolute hydroxyl radical density in diffuse atmospheric-pressure He–H_2O RF glow discharges. Additionally, using laser-induced fluorescence, Riès[10] measured the spatial distribution of hydroxyl radicals. The detection of these types of free radicals in liquids is typically conducted using electron paramagnetic resonance spectroscopy.[11]

In real-world applications, the challenge is to provide large-scale and uniform plasma treatment. One method of addressing this issue is to introduce plasma-activated water (PAW). In addition to efficient reactivity similar to the gas-phase plasma, PAW is able to effectively adapt to irregular shapes. This feature makes it possible to achieve

better effects in practical applications, for example, in the agriculture and food industry. PAW could play different roles during the different growth periods of crops. By affecting the activity of related enzymes, PAW has demonstrated the ability to enhance seed germination.[13] Additionally, PAW can serve as a nitrogen fertilizer for plant growth.[14,15] PAW is also used for postharvest treatment to extend the shelf life of food, owing to its excellent sterilization characteristics.[16,17]

There are two main methods for the preparation of PAW, which are mainly focused around two strategies: (1) discharge over the surface of the liquid and (2) discharge directly in the liquid. Various chemical reactions occurred at the plasma–liquid interface.[18] There are a variety of intermediate products created when preparing the PAW, which typically include nitric oxide radicals ($NO^{\bullet}$), nitrogen dioxide radicals ($NO_2^{\bullet}$), and hydroxyl radicals ($OH^{\bullet}$). These types of radicals have a short lifespan, typically of the order of 1 μs or less.[19,20] It is generally recognized that the durability of the efficiency of PAW is mainly regulated by its subsequent products, that is, nitrite (NO_2^-), hydrogen peroxide (H_2O_2), as well as other species.[21,22] Therefore, it is important to monitor and control the chemical composition of the PAW, and numerous methods have been tested. All current measurements are primarily based on spectrophotometry,[23–25] ion chromatography,[26,27] and electrochemistry analyzers.[22] When using spectrophotometry, signals from UV−Vis absorbance,[25,28] fluorescent labels,[23] or even the profile of spectrum[24] are detected and used to determine the concentrations. These instruments commonly have a complicated structure, at least containing some basic components, such as light source, light-dispersing unit, sample holder, detector, and readout device. Although there is a trend of developing highly portable spectrometers, the prices are still relatively high.[29–31] Ion-selective electrodes are typically electrochemistry sensors, which involve an invasive technique that requires accounting for the interference from other components. Current analysis tools do not respond well to the complex liquid environment in the PAW. All these methods rely heavily on complicated and expensive instruments, which typically limit their use in the laboratory. The existing detection methods are not suitable for outdoor working environments and are not capable of fast and online measurements.

With the advancements in photographic technology, high-quality and high-resolution images are readily available. Recently, the use of these color images for chemical analysis has attracted considerable attention.[32,33] Digital devices are able to effectively utilize the potential of chromogenic reactions. Digital colorimetry is based on the use of a computer-aided analysis of the color characteristics of an image to conduct qualitative or even quantitative measurements. There are multiple models for quantitatively defining color, of which the RGB system was designed specifically for digital devices, the CMYK model was developed for the printing industry, and the HSV or Lab model was developed to better imitate human vision. Image acquisition, storage, and processing are typically carried out on digital devices,[34] where the corresponding RGB model is commonly used. RGB intensities can be extracted from color images, where each parameter (Red–Green–Blue) covers 256 levels (0−255). In other words, there are 256^3 colors defined in the RGB system, and subtle differences in color can be effectively detected. Moreover, the values of other color parameters such as those from the CMYK, HSV, and Lab models can be derived with mapping from the RGB model. Millions of combinations of color components can guarantee precise detection and provide possibilities for widespread application.[35–37] Suzuki et al.[38] developed software that utilizes Lab values to determine iron and residual chlorine concentrations in water samples for use in water surveillance. Using RGB values as indicators, Lin et al.[39] proposed a novel method of detecting residual antibiotics for food safety control. Research conducted by Firdaus et al.[40] focused on the determination of chromium and iron concentrations to evaluate the degree of water contamination. Li et al.[41] developed a quantitative biomarker assay that uses microfluidic paper-based devices. Chemical analysis based on digital colorimetry has great potential in a wide variety of applications, such as in the food industry, environment monitoring, and clinical diagnosis.[42–48]

The goal of this study is to develop a simple and reliable method that employs digital colorimetry to detect long-lived chemical species in PAW. The absence of complicated and expensive instruments makes it an easy-to-use, time-effective, low-cost, and portable alternative. Nitrite (NO_2^-) and hydrogen peroxide (H_2O_2) were selected as the indicators of reactive nitrogen and reactive oxygen species in the PAW, respectively. First, we introduce the mechanisms and procedures for image acquisition, processing, and analysis. Subsequently, we present a method for determining the optimal detection strategy for NO_2^- and H_2O_2. Next, the results of the comparison between the proposed method and ordinary UV−Vis spectrometry are presented. Finally, we illustrate how this method integrates with a PAW generator for practical applications and discuss the optimization of the experimental conditions, the detection algorithms, and the performance comparison between the proposed method and the UV−Vis spectrometry.

2 | EXPERIMENTAL METHODS AND MATERIALS

2.1 | Chemicals and reagents

All solutions were prepared using distilled water throughout the experiments, unless otherwise stated. Sodium nitrite ($NaNO_2$; Sinopharm) was dissolved to prepare a NO_2^- standard stock solution, and H_2O_2 was diluted from a highly concentrated solution with a mass fraction of 30% (Sinopharm). To conduct the quantitative analysis, the Griess reagent (Sigma-Aldrich) was chosen as the colorimetric reagent that reacts with NO_2^- to form a violet azo compound.[49–51] Similarly, we used diluted sulfuric acid (H_2SO_4) to dissolve the appropriate amount of titanium sulfate ($Ti(SO_4)_2$; Sinopharm) to determine the concentration of H_2O_2.[52,53] The chromogenic reactions employed in the experiment should be carried out in an acidic environment and the pH should be maintained below 3. During the experiment, diluted hydrochloric acid (HCl) was used to control the acidity for the detection of NO_2^-, and H_2SO_4 was for H_2O_2. All reagents used in this investigation were of analytical grade and were used without further purification.

2.2 | Apparatus and software

A digital camera from a smartphone, with a resolution of 4000 × 3000 pixels, was employed in this study. The parameters of the smartphone are as follows: MEIZU M6 Note, Android 7.1.2, CPU Snapdragon 625, OctaCore 2.0 GHz, GPU Adreno 506, Screen (5.0 in., 1920 × 1080 [FHD]). We also built a light-emitting diode (LED) lightbox to ensure that all photographs had identical backgrounds, improving the experimental reproducibility. The LED (10 W) used here had a broad spectral band, covering ~400−700 nm (TKSP), and was ideal for illumination. The general procedure of the proposed method, based on digital colorimetry, is shown in Figure 1. The captured images were wirelessly transmitted to a computer and imported into MATLAB (R2017a) for image processing. The sample solution from either standard solution or PAW was mixed with the corresponding colorimetric reagent to complete the reaction. Subsequently, a quartz cuvette containing 2 ml of the mixture was placed into an LED lightbox with a uniform environment for image acquisition. Images of the chromogenic solution were then captured using the smartphone camera and transferred to a computer. The detailed photographic procedure is presented in Section 2.4. The images were processed using a computer for quantitative analysis. To verify the accuracy of the analysis, we also measured the species concentration using a UV–Vis spectrophotometer (SpectraMax M4 Multi-Mode Microplate Readers).

2.3 | Sample preparation

2.3.1 | Preparation of standard solutions

Both the proposed method and the existing method used as a reference to detect unknown solutions on the basis of standard solutions; therefore, we prepared both standard nitrite and hydrogen peroxide solutions for calibration. According to our calculations, we dissolved 345 mg of $NaNO_2$ in 50 ml of distilled water to obtain an NO_2^- solution with a concentration of 100 mM. Subsequently, this solution was

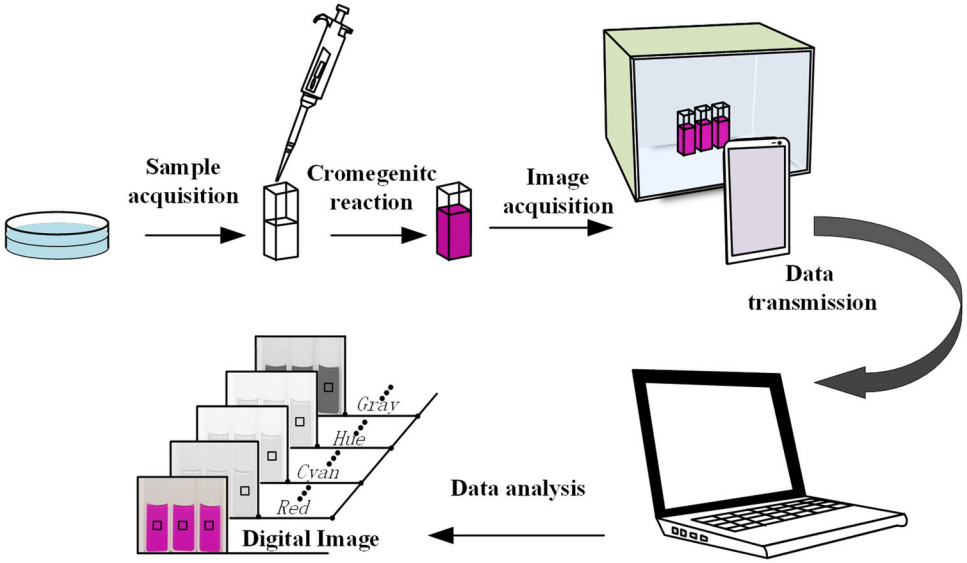

FIGURE 1 The general procedure of the proposed method, based on digital calorimetry

diluted to prepare a series of NO_2^- standard solutions, with concentrations ranging from 0 to 200 μM. A stock solution of H_2O_2 was prepared from a highly concentrated standard solution with a mass fraction of 30%. A series of H_2O_2 standard solutions was prepared for the calibration, with concentrations ranging from 0 to 20 mM.

2.3.2 | Preparation of PAW

To verify the efficiency of the proposed digital image processing method in PAW, two completely different plasma sources, a pin–plate discharge plasma and a surface microdischarge (SMD) plasma, were employed. The two plasma sources are both operating under an ambient air condition. The diagrams of these two devices and plasma discharge images are presented in Figure 2.

The experimental setup for PAW generation using the pin–plate discharge plasma is simple (Figure 2a). The powered electrode was made of a stainless-steel needle, with a diameter of 1.5 mm at the tip. A brass foil was immersed in the bottom of a Petri dish, connected to the external copper plate (ground electrode), to generate plasma between the needle and the surface of the solution. Furthermore, 10 ml of distilled water was added to the Petri dish (50 mm in diameter) for each plasma treatment. The gap between the tip of the needle and the surface of the solution was fixed at 5 mm. A positive DC source was used as the driving power. The high voltage between the electrodes fell from 10 to below 2 kV as the plasma ignited.

The structure of the SMD device (Figure 2b) can be divided into three main parts: a high-voltage electrode, an insulation medium, and a ground electrode. In this experiment, a brass cylinder with a diameter of 30 mm was used as the high-voltage electrode and a piece of stainless-steel mesh was used as the ground electrode. A 1-mm-thick ceramic plate was mounted between the two electrodes as a dielectric barrier. During treatment, a glass culture dish (50-mm diameter) with 10 ml of distilled water was placed at the bottom center of the chamber. The gap between the surface of the water and the ground electrode was fixed at 3 mm. The SMD was powered by a high-voltage AC source fixed at 11 kV (peak-to-peak), with a frequency of 8 kHz.

Due to the different productivities of NO_2^- and H_2O_2, the PAW for the measurements of the two species was prepared separately. We also varied the plasma exposure time to obtain different concentrations of PAW.

2.4 | Chromogenic reaction procedure and photographic preparation

To conduct the quantitative analysis, all samples were reacted completely with the colorimetric reagent before image acquisition. The chromogenic reaction time reserved for NO_2^- and H_2O_2 is 15 and 1 min, respectively. Detailed information is presented in Section 4.1. For NO_2^- detection, solutions were mixed with the Griess reaction assay in a ratio of 1:1 (v/v). In this chromogenic reaction, NO_2^- first reacts with sulfanilic acid to complete the diazo reaction. The diazonium compound then reacts with *N*-naphthyl-ethylenediamine to form a stable azo complex, which is indicated by a magenta color, with maximum absorbance at 540 nm. In this experiment, the indicator solution for detecting H_2O_2 was prepared by dissolving 3.75 g of $Ti(SO_4)_2$ using 100 ml of diluted sulfuric acid. In the presence of H_2SO_4, titanyl ions react with the H_2O_2 and form a yellow-colored peroxotitanyl complex, with a maximum absorbance at 407 nm. The mixing ratio between the sample solutions and dyes was 2:1 (v/v). Considering the complex composition of the PAW, it is necessary to eliminate interference from other components. In particular, H_2O_2 can be decomposed by NO_2^- under acidic conditions. To eliminate this interference, sodium azide (NaN_3) was added during the detection of H_2O_2.[50]

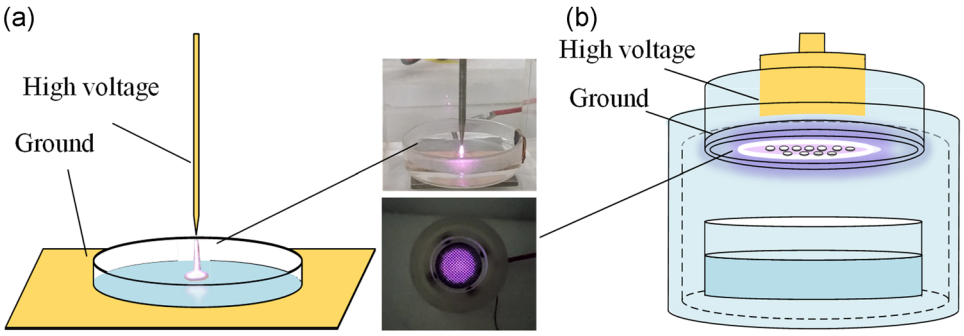

FIGURE 2 The experimental setups for plasma-activated water generation. (a) The pin–plate discharge plasma and (b) the surface microdischarge plasma

The quartz cuvette (1 × 1 × 4 cm), containing 2 ml of the mixture, was then put into the LED lightbox to standardize the external conditions, including the shooting distance, shooting angle, and illumination, during digital photography. During all experiments, the camera settings were held constant. For each sample, the procedure was performed three times.

3 | RESULTS

3.1 | Quantification of digital images

Figures 3a and 3b show typical images of chromogenic solutions of NO_2^- and H_2O_2, respectively. After reacting with the colorimetric reagent, the NO_2^- solution turned into a typical magenta color and the H_2O_2 solution turned yellow. The color of the sample solution changes as the concentration is changed in both cases. With the help of digital image processing, these dynamic changes in the color are able to be quantitatively detected. To obtain as much color information over the entire concentration range as possible, and enable a more accurate analysis, color parameters, including RGB, HSV, CMYK, and Lab, for each pixel were extracted using MATLAB. To achieve a high level of stability, an area of 100 × 100 pixels was selected, where the average value of each parameter was used as the final signal. The RGB system is the most commonly used color model, as such, and we selected RGB values as representatives of color parameters for demonstration. As shown in Figure 3c,d, RGB values change dynamically with the concentration. In the case of NO_2^-, both the R and B channels show a parabolic trend, increasing initially to a maximum before decreasing. The G value monotonically decreased as the concentration increased. For the H_2O_2 solutions, the R component again shows a parabolic trend. The working curves of the G and B components have local linearity characteristics, both of which are saturated at either low or high concentrations. Other color parameters also showed concentration dependence (not shown here), and all data was stored for further analysis.

3.2 | Determining the detection strategy

According to the results in Figure 3, it is clear that both the overall color and the individual color components are dependent on the species concentration. The dynamic changes in the different color parameters contain significant information regarding the solution. To deduce the concentration, the working curves of the color parameters with respect to concentration were analyzed in detail.

Polynomial and exponential fitting are the most common methods of regression analysis and are typically applied to the working curve. The monotonicity, linearity, and sensitivity (slope or first-order derivative) of the working curve are capable of significantly affecting the effectiveness of the regression analysis. Given the problems with overfitting and error accumulation, linear regression is the best choice to provide a reliable and

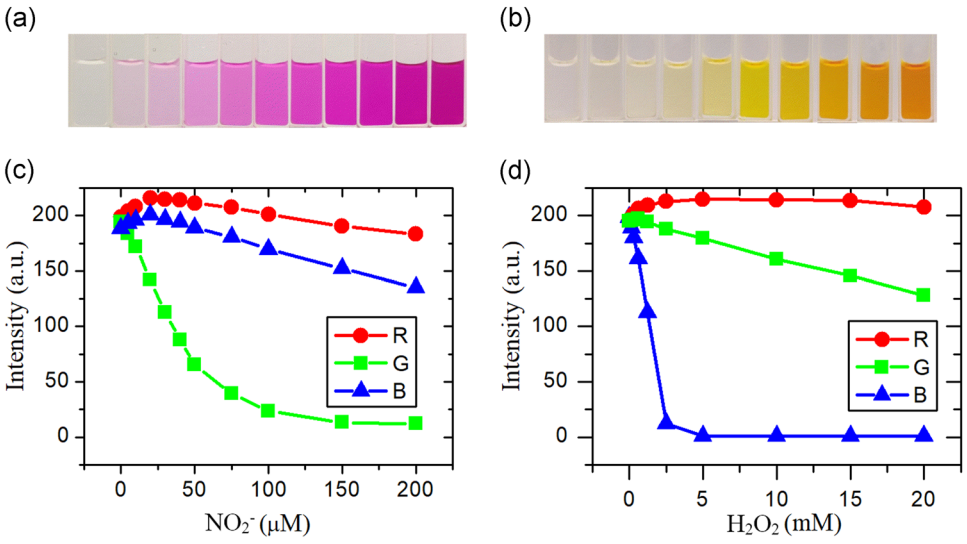

FIGURE 3 Typical images of chromogenic solutions. (a) The NO_2^- standard solutions (0–200 μM) indicated by the magenta color, (b) the H_2O_2 standard solutions (0–20 mM) indicated by the yellow color, (c) RGB values versus NO_2^- concentration, and (d) RGB values versus H_2O_2 concentration

easy-to-use prediction. Once the regression equation is determined, the accuracy of the prediction is largely reflected in the correlation coefficient (R^2). However, it was not feasible to directly perform linear regression on the working curves in this experiment. In the cases of both NO_2^- and H_2O_2, all of the color components (RGB, CMYK, HSV, and Lab) exhibited a number of problems, including low sensitivity, nonlinearity, non-monotonicity, and local saturation, over the entire testing range.

To address these issues, a strategy of combining different color parameters for piecewise fitting was developed. The flowchart of the strategy for concentration detection is shown in Figure 4. After processing the tested image, the concentration is initially determined by a selected component, R1. According to the comparison with threshold A, the concentration is finally checked by R2 or R3 components. The selection of color components for analysis is based on their respective monotonic concentration range, rather than the entire range. Component R1 is selected to estimate the initial concentration and should remain monotonic over the entire concentration range. The other two components (R2 and R3) are responsible for precise predictions and require good linearity and sensitivity over their respective ranges. Threshold A is finally determined according to the selected components. This method combines information from multiple components and is able to expand the linear detection range and improve the sensitivity.

The following refers to the strategic decision processes for NO_2^- and H_2O_2, shown in Figure 5, for a more detailed explanation. For NO_2^- detection, the L component, from the Lab color system, remains monotonic over the entire detection range (0–200 μM) but loses linearity (Figure 5a). The G component shows good sensitivity and excellent linearity over the range of 0–40 μM (Figure 5b), and the B component exhibits a linear decrease in the high concentration range (Figure 5c). The two-step detection is performed as follows: first, exponential fitting of the L component deduces the initial concentration; then, if the initial measurement falls into the low-concentration range (<40 μM), the G component is used for precise detection, otherwise, the B component is used. Similarly, the chromatic parameters for H_2O_2 detection were screened out: the L component for initial detection (Figure 5d), the B component for the low-concentration range (Figure 5e), and the G component for the high-concentration range (Figure 5f).

3.3 | Performance test on configured solution and PAWs

To verify the accuracy of the proposed method, we first tested a configured solution of both NO_2^- and H_2O_2. Testing samples were chosen from the standard series. Once selected, the concentration of the target sample

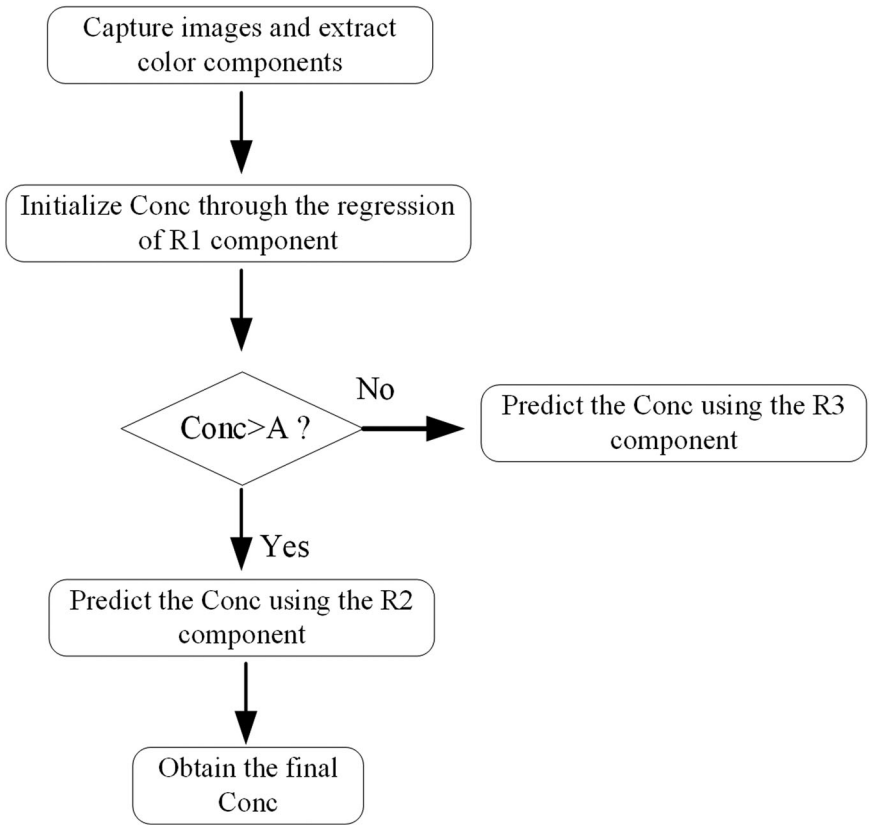

FIGURE 4 Flowchart of detection strategy. A is the threshold, R1 component charges for the global detection range, R2 works in a high-concentration range, and R3 in a low-concentration range

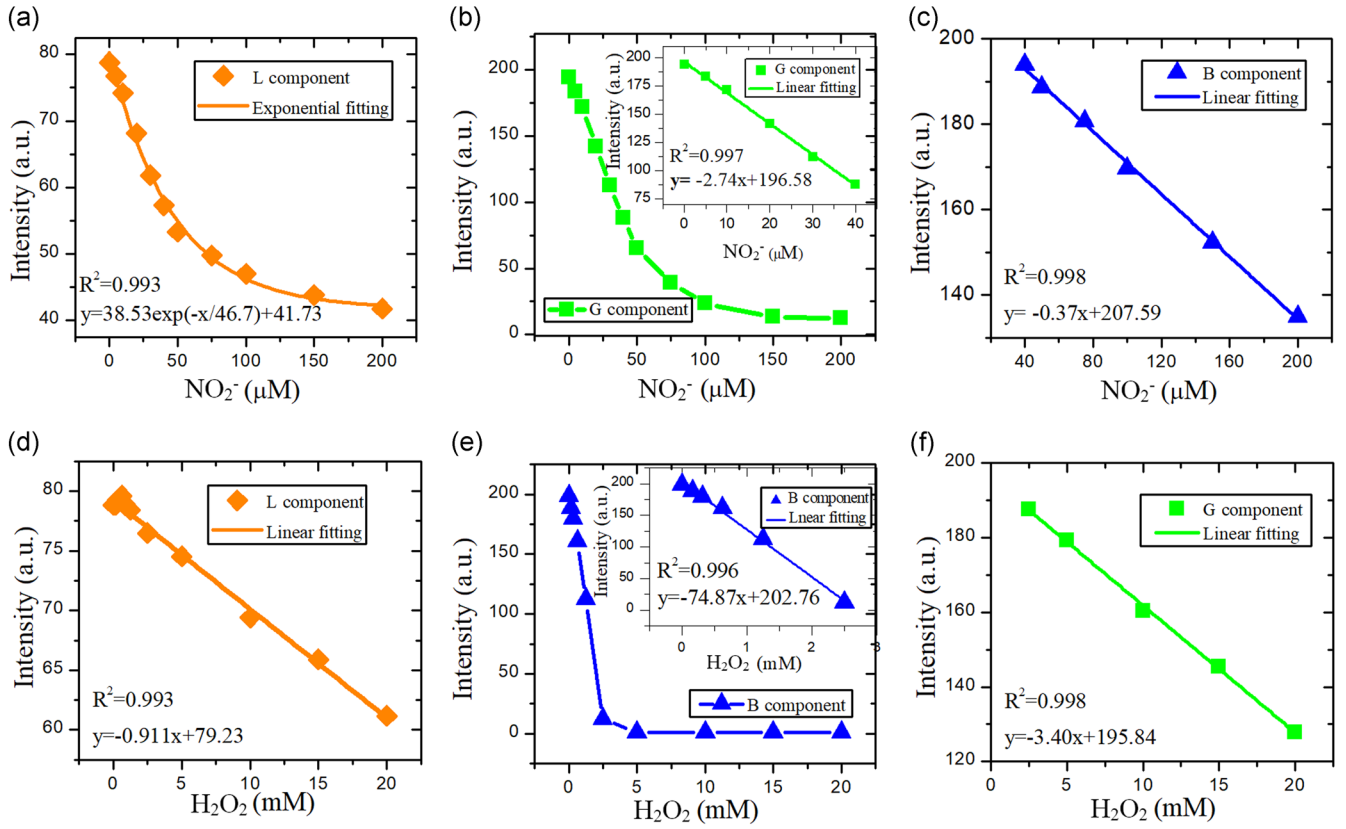

FIGURE 5 Regression analysis on working curves. (a) L component in NO_2^- (0–200 μM), (b) G component in NO_2^- (0–40 μM), (c) B component in NO_2^- (40–200 μM), (d) L component in H_2O_2 (0–20 mM), (e) B component in H_2O_2 (0–2.5 mM), and (f) G component in H_2O_2 (2.5–20 mM)

remained unknown, whereas the other samples were used for prediction. To compare the analytical performance of the digital colorimetry and UV–Vis spectrometry methods, all tests were limited to a reasonable range of 0–150 μM for NO_2^- and 0–5 mM for H_2O_2. Both of the absorption spectrum signals (optical depth of 1 cm) were collected, as shown in Figure 6a,b. Concentrations of 20, 40, 75, and 100 μM from the standard solution were chosen for NO_2^- and concentrations of 0.625, 1.25, 2.5, and 5 mM were used for H_2O_2. The results from these tests are presented in Figure 6c,d. The analytical performance of the proposed method based on digital colorimetry was comparable to that of the UV–Vis method. Compared with theoretical value, both methods reach a level of accuracy with an absolute error (AE) <6 μM and relative error (RE) within 6% for NO_2^-. In the case of H_2O_2, the maximum AE is 0.2 mM and RE is approximately 8%.

After verifying the feasibility of the proposed method using the standard solutions, we also analyzed the species concentrations in PAWs generated by pin–plate discharge and SMD. The absolute concentration was measured using both the proposed method and UV–Vis spectrometry. As can be seen from Figure 7, both NO_2^- and H_2O_2 accumulate in PAW as the plasma treatment time is increased in both cases. The production of the target species from the SMD plasma is relatively milder than that from the pin–plate spark discharge. The productivity of NO_2^- and H_2O_2 in SMD PAW is similar to the results reported by Traylor et al.[22] In the case of a pin–plate discharge, the concentrations of both the NO_2^- and H_2O_2 are higher than those reported by Anderson et al.,[50] which may be due to the different amounts of energy dissipated into the plasma. For the PAW prepared by SMD, the productivity of H_2O_2 is much smaller than that of NO_2^-. To avoid having an extremely low concentration, causing a failure in detection, we extended the plasma exposure time up to 30 min for H_2O_2 detection. By using pin–plate spark discharge, the generation efficiency of the two compounds is greatly improved and the productivity of H_2O_2 is almost equal to that of NO_2^-.

Unlike the analysis of the standard solutions, there are no so-called theoretical concentrations in the PAW for comparison. Instead, we compared the results from the proposed method and the UV–Vis method. For the detection of NO_2^-, the AE is <8 μM and RE is within 10% in the PAWs from the two different plasma sources (Figure 7a1,b1). The maximum AE for the detection of H_2O_2 is approximately 0.17 mM with an RE of 10% (Figure 7a2,b2). The results from the two methods

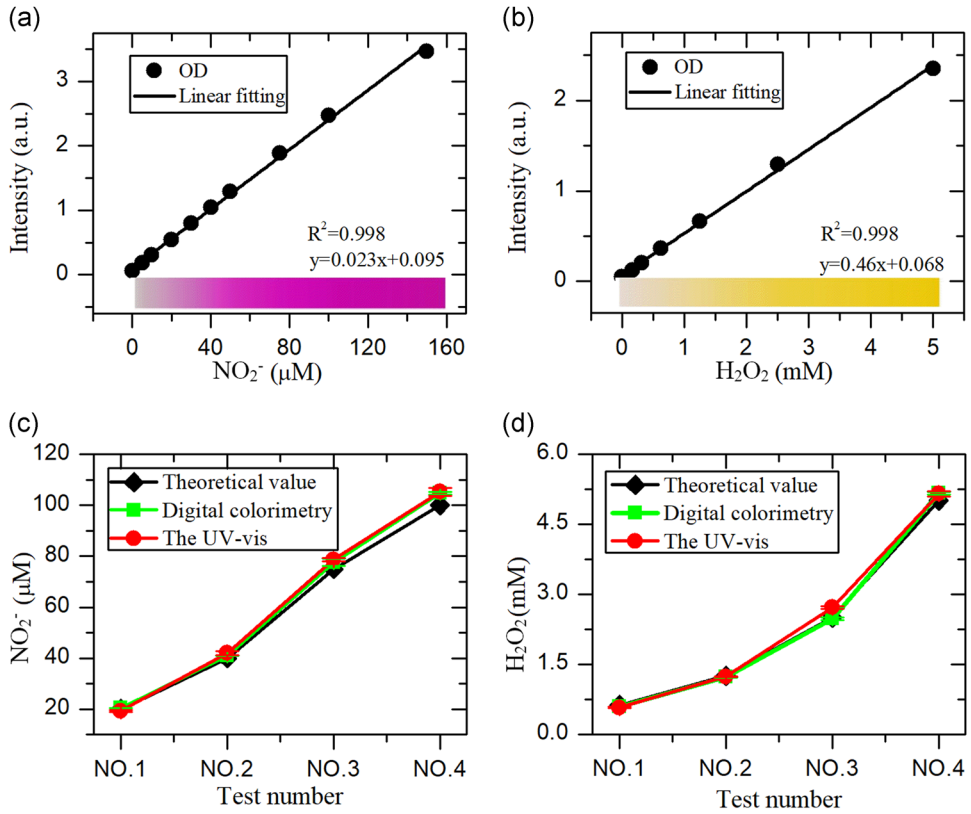

FIGURE 6 Detection performance using the configured solution. (a) Detection range for testing in NO_2^- (0–150 μM), (b) detection range for testing in H_2O_2 (0–5 mM), (c) detection of NO_2^- in the configured solution, and (d) detection of H_2O_2 in the configured solution

are consistent within a reasonable range. It should be noted that there is no doubt that detection errors exist for both methods, and the inconsistency is mainly due to the accumulation of errors from the two measurement methods. The accuracy can also be improved by eliminating the interference from external factors and improving the algorithms.

4 | DISCUSSION

For practical applications in real-world environments, the ability to detect the specific contents of the PAW is important. The effectiveness of the PAW is mainly regulated by the concentrations of long-lived oxygen and nitrogen species (H_2O_2, NO_2^-, NO_3^-, etc.). In agricultural applications, the H_2O_2 in the PAW is responsible for enhancing seed generation.[13] Additionally, the long-lived nitrogen species (NO_2^-, NO_3^-) in the PAW are assimilated into organic compounds in the soil, and they subsequently act as a fertilizer.[14] The existing methods of analyzing PAW require expensive and complicated equipment, such as a spectrometer or chromatograph, which are not suitable for outdoor operation. The proposed method based on digital colorimetry, however, has a simple structure and could be well adapted to various working environments, such as in a greenhouse or a food processing chain. In addition, the proposed method can be easily employed in the real world rather than being limited to laboratory use. As shown in Figure 8, we are able to integrate the detecting module of the proposed method directly onto a PAW generator. This all-in-one device includes a section for automatic sampling, the ability to acquire images, and a control panel. According to the set sampling time, the device automatically samples and prepares for chromogenic reaction. A camera integrated into the device is designed for capturing the digital images of the colored solution. All the procedures and data processing will be done through the control panel. Given these features, when the PAW generator is in operation, the concentration of the target species can be read directly from the display on the screen of the control panel.

4.1 | Optimization of experimental conditions

The proposed method is based on the analysis of digital images and, as such, any factor affecting image

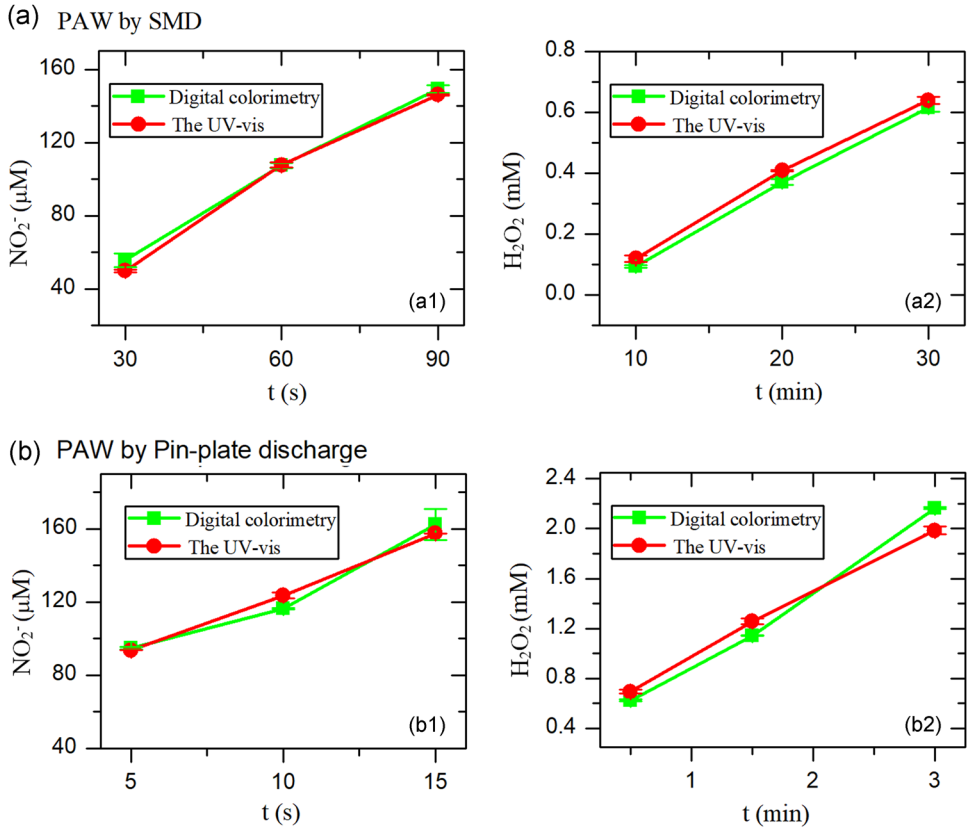

FIGURE 7 Detection performance in plasma-activated water (PAW). (a) Detection results of NO_2^- (a1) and H_2O_2 (a2) in PAW prepared using the surface microdischarge (SMD); (b) detection results of NO_2^- (b1) and H_2O_2 (b2) in PAW prepared using the pin–plate discharge plasma

acquisition should be optimized. In this study, an acrylic LED lightbox was introduced to provide a uniform white background and consistent illumination. During each acquisition, the camera was adjusted to focus on the sample cells at a fixed distance of 20 cm. Appropriate time was reserved for the color reaction to complete before the image was acquired. If sufficient time is not reserved, the reaction will be incomplete; however, if the reaction is allowed to run too long, it may result in discoloration. The amount of time required for the color

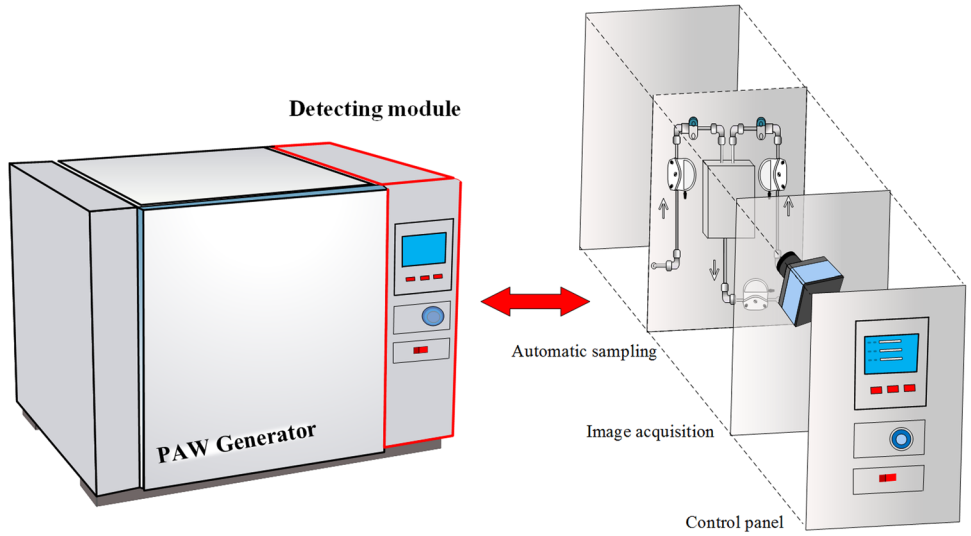

FIGURE 8 Plasma-activated water (PAW) generator equipped with the detecting module based on the proposed method

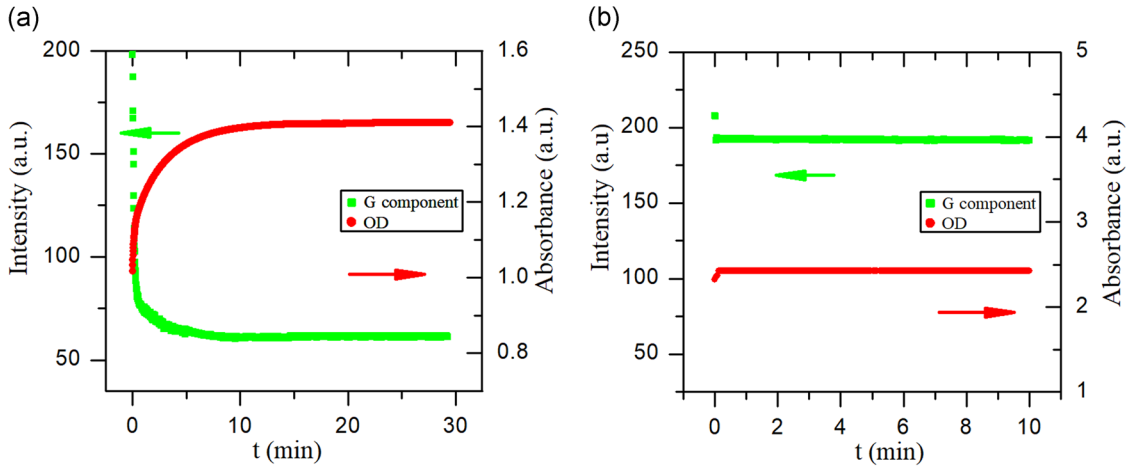

FIGURE 9 Evolution of G component and optical density (OD) value versus time in (a) 50-μM nitrite chromogenic reaction and (b) 5-mM hydrogen peroxide chromogenic reaction

reaction was determined on the basis of two metrics: the spectral signal (optical density [OD]) generation and the color signal (G component) development, as shown in Figure 9. Both signals for the NO_2^- are stable after approximately 10 min, whereas they become stable within 30 s for H_2O_2. Certainly, this amount of time is dependent on the manufacturer of the colorimetric reagent. Additionally, both of the colored compounds are relatively stable and are able to remain constant for several hours.[49,52] To achieve the optimal results, the images were not captured until after reacting for 15 min for the NO_2^- solution and 1 min for the H_2O_2 solution. To avoid fading of the colored complex, all processes were performed within 60 min of starting.

The liquid environment also requires a strict control. Diluted HCl or H_2SO_4 was used in this study to maintain the acidic environment for chromogenic reaction. For the pH value below 3, the G component and OD value for both NO_2^- and H_2O_2 detection remain constant, as given in Supporting Information Materials S1. For a better linear curve fitting, the pH value was kept below 3 during all the chromogenic reactions.

Both the proposed method and the UV–Vis method are based on chromogenic reactions; thus, the choice of colorimetric reagent is also important. The selection of the appropriate color reagents can result in significantly improved results. Besides detecting H_2O_2 with $Ti(SO_4)_2$, metavanadate can also be used, which is indicated by a red-orange color with a maximum absorbance at 450 nm.[54] Other long-lived species in PAW, such as NO_3^-, could also be detected using a method based on digital colorimetry. NO_3^- detection could be performed by reaction with 2,6-dimethylphenol, indicated by an orange color with peak absorption at 340 nm.[55]

4.2 | Improvement of detection algorithms

In digital colorimetry, it is common to extract multiple color parameters (including RGB, CMYK, HSV, and Lab) and then select the one with the best linearity over the entire concentration range for analysis.[35,36,40] However, this selection depends on both the detecting substance and the concentration range tested. Although there may be numerous candidates to choose from, there is no guarantee that an appropriate parameter for linear regression analysis exists for the entire detection range. In this study, a strategy of combining multiple components was adopted. The detection range was divided into different blocks according to the threshold, and the optimal components were selected for analysis within their respective linear ranges. This strategy guarantees that linear regression can be effectively utilized in this study, expands the linear detection range, and maintains excellent sensitivity. Nevertheless, the algorithm can still be further improved.

Unlike linear regression on a single signal, multiple regression analysis is able to provide comprehensive information for a thorough analysis. Furthermore, extensive dynamic color information was obtained during the experiment, which could serve as a database for machine learning. Due to its significant advantages in data processing, we may also be able to use support vector machine neural networks for further improvement.

4.3 | Performance comparison

For the UV–Vis method, nonlinearity caused by signal saturation or excessive signal strength can invalidate the detection. However, the proposed method is based on the

TABLE 1 The analytical performance comparison between digital colorimetry and the UV−Vis

Analyte	Detection methods	Sensitivity (auL/μmol)	Working range	Linearity	LOD	Resolution
NO_2^-	The UV−Vis	0.023	0−150 μM	0.998	3.14 μM	0.043 μM
	This method	2.74/0.37	0−200 μM	0.997/0.998	1.52 μM	0.36/2.70 μM
H_2O_2	The UV−Vis	0.46	0−5 mM	0.998	0.12 mM	0.00217 mM
	This method	74.87/3.4	0−20 mM	0.996/0.998	0.09 mM	0.0134/0.294 mM

Note: A/B means the values in different working ranges decided by the linear range of different color components.
Abbreviation: LOD, limit of detection.

analysis of color characteristics, which means that as long as the color information changes, it will still be within the effective range. We performed additional experiments to compare the detection range of the proposed method and the common UV−Vis absorption method (SpectraMax M4 Multi-Mode Microplate Readers were used in this study), whose detailed results are presented in Supporting Information Materials S2. Under the same standard optical depth (1 cm), for NO_2^- detection, the range of the proposed method is from 0 to 200 μM and the detection based on UV−Vis is limited to a range of 0−150 μM. For H_2O_2, the range of the proposed method is from 0 to 20 mM; however, the detection based on UV−Vis is limited to a range of 0−5 mM.

A more detailed analytical performance comparison between digital colorimetry and the UV−Vis is listed in Table 1. The calculation of the parameters can be found in Supporting Information Materials S3. From the data, we can observe that the proposed method has better performance regarding sensitivity, working range, and LOD than the SpectraMax M4 Multi-Mode Microplate Readers in the detection of NO_2^- and H_2O_2 conducted in this study. Meanwhile, the linearity over the whole detection range is similar. Although the resolution of the proposed method is not as good as that of the SpectraMax M4 Multi-Mode Microplate Readers, however, it is necessary to point out that the SpectraMax M4 is much more expensive. The resolution of the proposed method may be improved by improving the detection algorithm. However, if compared with a low-cost spectrometer, the performance parameters should be outstanding. In addition, compared with the detection range, the resolution is good enough for measurements in out-lab use.

5 | CONCLUSION

A method based on digital colorimetry was developed and proposed for easy and low-cost chemical analysis of PAW, which also enables online and portable measurements. The proposed method only requires a smartphone camera to capture images of the PAW mixed with a colorimetric reagent and is able to analyze the solution remotely on a computer or directly on the smartphone, without sophisticated and expensive instruments. We adopted the piecewise fitting method to conduct linear regression analyses in different concentration ranges, according to the specific color information of the different detecting species. The results of this method in detecting NO_2^- and H_2O_2 in the PAW prepared from pin−plate discharge and SMD were similar to the results obtained using the ordinary UV−Vis spectra. The proposed method can also be extended to the detection of other chemistries, as long as there are suitable colorimetric reagents. It also results in better performance regarding LOD, working range, and sensitivity as compared with the UV−Vis method. Any improvement in the detection algorithms, such as the adoption of machine learning, may improve accuracy. Compared with ordinary spectrometry, which is only able to acquire signals at a specific point, the proposed method can easily obtain information from all aspects, providing the prospect for spatial−temporal distribution analysis. Further work will be focused on the spatiotemporal evolution of long-lived species to achieve in situ and real-time diagnostics of PAW.

ACKNOWLEDGMENTS

The authors are grateful for financial support from the Independent Innovation Fund of Huazhong University of Science and Technology (No. 2018KFYYXJJ071) and the National Natural Science Foundation of China (No. 51907076).

ORCID

Zilan Xiong http://orcid.org/0000-0003-1095-3959

REFERENCES

[1] M. G. Kong, G. Kroesen, G. Morfill, T. Nosenko, T. Shimizu, J. Van Dijk, J. L. Zimmermann, *J. Phys.* **2009**, *11*, 115012.
[2] C. Lu, J. Dai, N. Dong, Y. Zhu, Z. Xiong, *Plasma Processes Polym.* **2020**, *17*, 1069. https://doi.org/10.1002/ppap.202000100
[3] R. Morent, N. De Geyter, T. Desmet, P. Dubruel, C. Leys, *Plasma Processes Polym.* **2011**, *8*, 171.

[4] H. Zhou, Q. Xie, H. Ruan, G. An, G. Wu, X. Yang, Y. Zhang, *Polym. Compos.* **2020**, *41*, 2881. https://doi.org/10.1002/pc.25584
[5] R. Thirumdas, A. Kothakota, U. Annapure, K. Siliveru, R. Blundell, R. Gatt, V. P. Valdramidis, *Trends Food Sci. Technol.* **2018**, *77*, 21.
[6] M. Ito, T. Ohta, M. Hori, *J. Korean Phys. Soc.* **2012**, *60*, 937.
[7] S. Reuter, J. S. Sousa, G. D. Stancu, J. P. H. van Helden, *Plasma Sources Sci. Technol.* **2015**, *24*, 054001.
[8] P. Bruggeman, G. Cunge, N. Sadeghi, *Plasma Sources Sci. Technol.* **2012**, *21*, 035019.
[9] Y. Kasashima, T. Brenner, K. Vissing, *Plasma Processes Polym.* **2020**, e2000077. https://doi.org/10.1002/ppap.202000077
[10] D. Riès, *Ph.D. Thesis*, Université d'Orléans **2014**.
[11] H. Jablonowski, R. Bussiahn, M. U. Hammer, K. D. Weltmann, T. von Woedtke, S. Reuter, *Phys. Plasmas* **2015**, *22*, 122008.
[12] S. Kelly, M. M. Turner, *Plasma Sources Sci. Technol.* **2014**, *23*, 065013.
[13] N. Puač, N. Škoro, K. Spasić, S. Živković, M. Milutinović, G. Malović, Z. L. Petrović, *Plasma Processes Polym.* **2018**, *15*, 1700082.
[14] D. P. Park, K. Davis, S. Gilani, C. A. Alonzo, D. Dobrynin, G. Friedman, G. Fridman, *Curr. Appl. Phys.* **2013**, *13*, S19.
[15] S. Zhang, A. Rousseau, T. Dufour, *RSC Adv.* **2017**, *7*, 31244.
[16] R. Ma, S. Yu, Y. Tian, K. Wang, C. Sun, X. Li, J. Fang, *Food Bioprocess Technol.* **2016**, *9*, 1825.
[17] Y. Xu, Y. Tian, R. Ma, Q. Liu, J. Zhang, *Food Chem.* **2016**, *197*, 436.
[18] P. J. Bruggeman, M. J. Kushner, B. R. Locke, J. G. Gardeniers, W. G. Graham, D. B. Graves, D. F. Rivas, *Plasma Sources Sci. Technol.* **2016**, *25*, 053002.
[19] H. S. Kim, K. C. Wright, I. W. Hwang, D. H. Lee, A. Rabinovich, A. Fridman, Y. I. Cho, *Int. Commun. Heat Mass Transfer.* **2013**, *42*, 5.
[20] T. He, D. Liu, H. Xu, D. Xu, D. Li, Q. Li, M. G. Kong, *J. Phys. D: Appl. Phys.* **2016**, *49*, 205204.
[21] B. R. Locke, P. Lukes, J. L. Brisset, *Plasma Chemistry and Catalysis in Gases and Liquids*, Wiley-VCH Verlag GmbH & Co. KGaA, Germany **2012**, p. 185.
[22] M. J. Traylor, M. J. Pavlovich, S. Karim, P. Hait, Y. Sakiyama, D. S. Clark, D. B. Graves, *J. Phys. D: Appl. Phys.* **2011**, *44*, 472001.
[23] D. Dobrynin, *Ph.D. Thesis*, Drexel University (Philadelphia, PA) **2011**.
[24] J. S. Oh, E. J. Szili, K. Ogawa, R. D. Short, M. Ito, H. Furuta, A. Hatta, *Jpn. J. Appl. Phys.* **2017**, *57*, 0102B9.
[25] M. Naïtali, G. Kamgang-Youbi, J. M. Herry, M. N. Bellon-Fontaine, J. L. Brisset, *Appl. Environ. Microbiol.* **2010**, *76*, 7662.
[26] E. Dolezalova, P. Lukes, *Bioelectrochemistry* **2015**, *103*, 7.
[27] R. Laurita, D. Barbieri, M. Gherardi, V. Colombo, P. Lukes, *Clin. Plasma Med.* **2015**, *3*, 53.
[28] Z. Stara, F. Krčma, *Czech. J. Phys.* **2004**, *54*, C1050.
[29] D. González-Morales, A. Valencia, A. Díaz-Nuñez, M. Fuentes-Estrada, O. López-Santos, O. García-Beltrán, *Sensors* **2020**, *20*(*3*), 906.
[30] A. B. D. Nandiyanto, R. Zaen, R. Oktiani, A. G. Abdullah, L. S. Riza, *Telkomnika* **2018**, *16*(*2*), 580.
[31] D. A. Czegan, D. K. Hoover, *J. Chem. Educ.* **2012**, *89*, 304.
[32] W. Wu, J. P. Allebach, M. Analoui, *J. Imaging Sci. Technol.* **2000**, *44*, 267.
[33] E. V. Schults, O. V. Monogarova, K. V. Oskolok, *Moscow Univ. Chem. Bull.* **2019**, *74*, 55.
[34] R. C. Gonzalez, R. E. Woods, S. L. Eddins, *Digital Image Processing Using MATLAB*, Pearson Education, India **2004**.
[35] P. Masawat, A. Harfield, N. Srihirun, A. Namwong, *Anal. Lett.* **2017**, *50*, 173.
[36] J. Wongthanyakram, P. Masawat, *Anal. Lett.* **2019**, *52*, 550.
[37] I. S. Porto, J. H. S. Neto, L. O. dos Santos, A. A. Gomes, S. L. Ferreira, *Microchem. J.* **2019**, *149*, 104031.
[38] Y. Suzuki, M. Endo, J. Jin, K. Iwase, M. Iwatsuki, *Anal. Sci.* **2006**, *22*, 411.
[39] B. Lin, Y. Yu, Y. Cao, M. Guo, D. Zhu, J. Dai, M. Zheng, *Biosens. Bioelectron.* **2018**, *100*, 482.
[40] M. L. Firdaus, W. Alwi, F. Trinoveldi, I. Rahayu, L. Rahmida, K. Warsito, *Procedia Environ. Sci.* **2014**, *20*, 298.
[41] X. Li, J. Tian, W. Shen, *Anal. Bioanal. Chem.* **2010**, *396*, 495.
[42] *Proc. Workshop Fire Design of Concrete Structures: What now? What next?* (Eds: P. G. Gambarova, R. Felicetti, A. Meda, P. Riva), Milan University of Technology, Milan, Italy **2004**.
[43] C. X. Yang, X. Y. Sun, B. Liu, H. T. Lian, *Chin. J. Anal. Chem.* **2007**, *35*, 850.
[44] V. V. Apyari, S. G. Dmitrienko, Y. A. Zolotov, *Moscow Univ. Chem. Bull.* **2011**, *66*, 32.
[45] J. P. Devadhasan, S. Kim, *Anal. Chim. Acta* **2015**, *858*, 55.
[46] M. R. Ioan, *Nucl. Eng. Technol.* **2018**, *50*, 519.
[47] A. Choodum, W. Sriprom, W. Wongniramaikul, *Spectrochim. Acta, Part A* **2019**, *208*, 40.
[48] A. Lopez-Molinero, V. T. Cubero, R. D. Irigoyen, D. S. Piazuelo, *Talanta* **2013**, *103*, 236.
[49] M. B. Shinn, *Ind. Eng. Chem., Anal. Ed.* **1941**, *13*, 33.
[50] C. E. Anderson, N. R. Cha, A. D. Lindsay, D. S. Clark, D. B, *Plasma Chem. Plasma Process.* **2016**, *36*, 1393.
[51] J. Sun, X. Zhang, M. Broderick, H. Fein, *Sensors* **2003**, *3*, 276.
[52] P. Lukes, E. Dolezalova, I. Sisrova, M. Clupek, *Plasma Sources Sci. Technol.* **2014**, *23*, 015019.
[53] M. Mori, M. Shibata, E. Kyuno, S. Ito, *Bull. Chem. Soc. Jpn.* **1956**, *29*, 904.
[54] C. Van Gils, S. Hofmann, B. K. H. L. Boekema, R. Brandenburg, P. J. Bruggeman, *J. Phys. D: Appl. Phys.* **2013**, *46*, 175203.
[55] K. Oehmigen, M. Hähnel, R. Brandenburg, C. Wilke, K. D. Weltmann, T. Von Woedtke, *Plasma Processes Polym.* **2010**, *7*, 250.

SUPPORTING INFORMATION

Additional Supporting Information may be found online in the supporting information tab for this article.

How to cite this article: Zou Z, Han R, Lu C, Xiong Z. Detection of long-lived species in plasma-activated water, based on digital colorimetry. *Plasma Process Polym*. 2020;e2000139. https://doi.org/10.1002/ppap.202000139